Supporting Information

Z-Scheme interface engineering in bimetallic sulfide sonozymes to dismantle tumor antioxidant defenses for ferroptosis-driven sono-immunotherapy

Yang Yang[a,1], Xiuwei Wu[a,1], Zhenlin Zhang[b], Dengyu Pan[b], Bijiang Geng[b,*], Yunsheng Cheng[c,*]

a Department of Oncology, The Second Affiliated Hospital of Anhui Medical University, Hefei, Anhui 230601, China

[b] School of Environmental and Chemical Engineering, Shanghai University, Shanghai 200444, China

c Department of General Surgery, Second Affiliated Hospital of Anhui Medical University, Hefei, Anhui 230601, China

[1] These authors contributed equally to this work.

* Corresponding authors.

E-mail addresses: bjgeng1992@shu.edu.cn (B. Geng); chengyunsheng@ahmu.edu.cn (Y. Cheng)

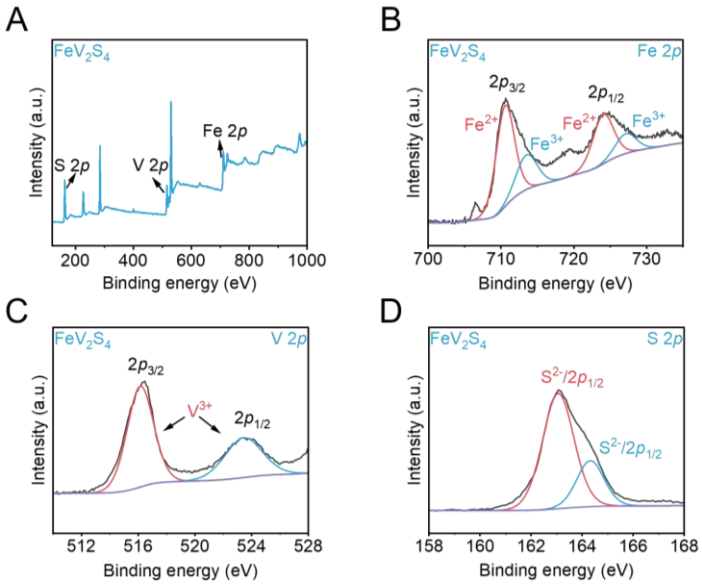


Figure S1. Survey XPS (A), high-resolution Fe 2*p* (B), V 2*p* (C) and S 2*p* (D) spectra of FeV_2S_4.

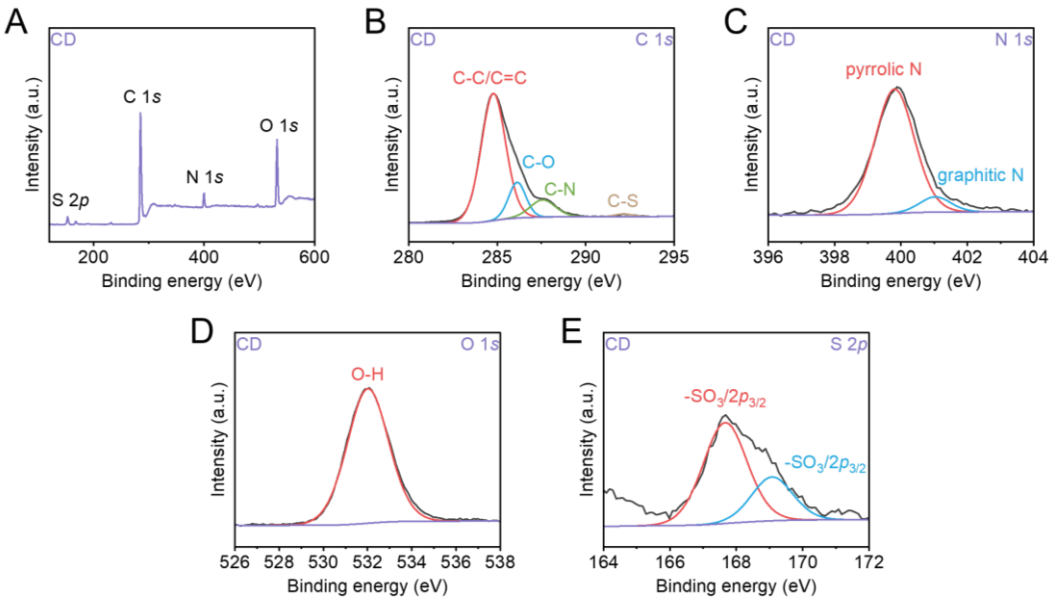


Figure S2. Survey XPS (A), high-resolution C 1*s* (B), N 1*s* (C), O 1*s* (D) and S 2*p* (E) spectra of CD.

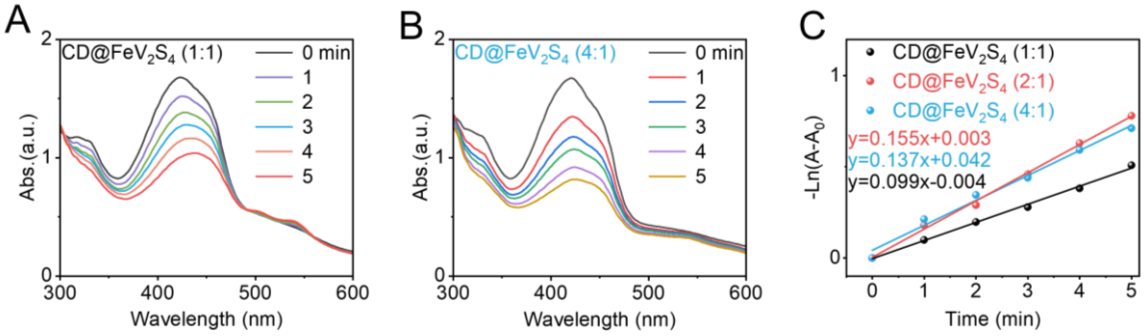


Figure S3. Comparison of the sonodynamic activity of CD@H-RuO_2 prepared at different mass ratios

of CD to FeV_2S_4.

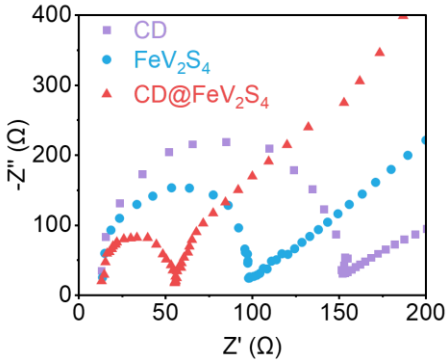


Figure S4. The impedance spectra of CD@FeV_2S_4, FeV_2S_4, and CD.

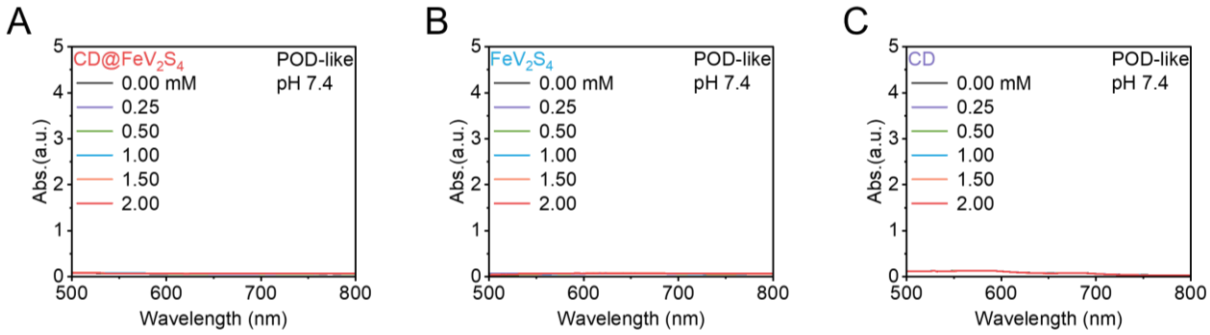


Figure S5. Measurements of the POD-like activity of CD@FeV_2S_4 (A), FeV_2S_4 (B), and CD (C) under pH 7.4.

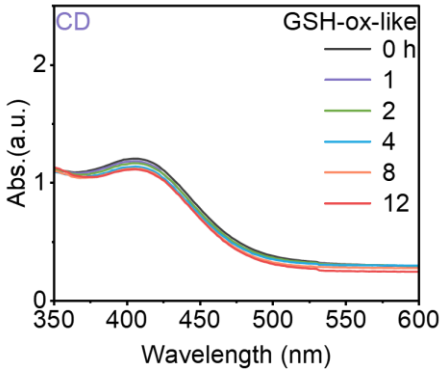


Figure S6. Measurements of the GSH-ox-like activity of CD.

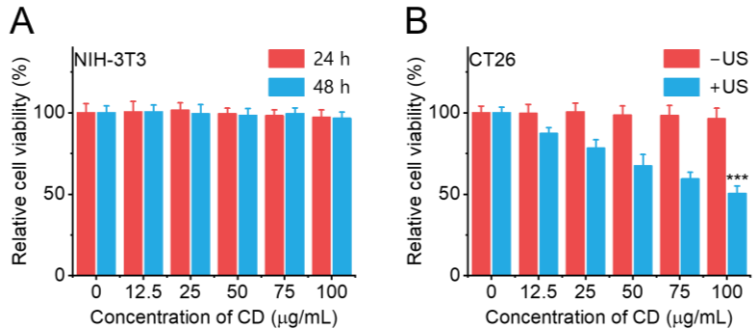


Figure S7. Cytotoxicity assessment of CDs towards NIH-3T3 cells (A) and CT26 cells with or without US (B). Data are presented as the mean ± SD. (n = 6). ***p < 0.001.

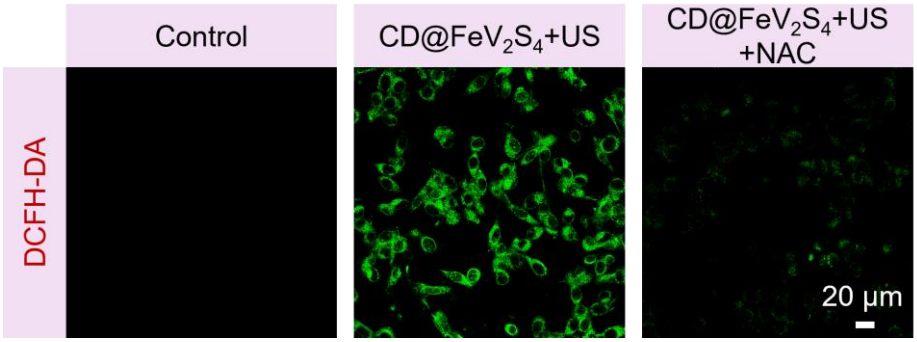


Figure S8. ROS staining assay of CT26 cells after different treatments.

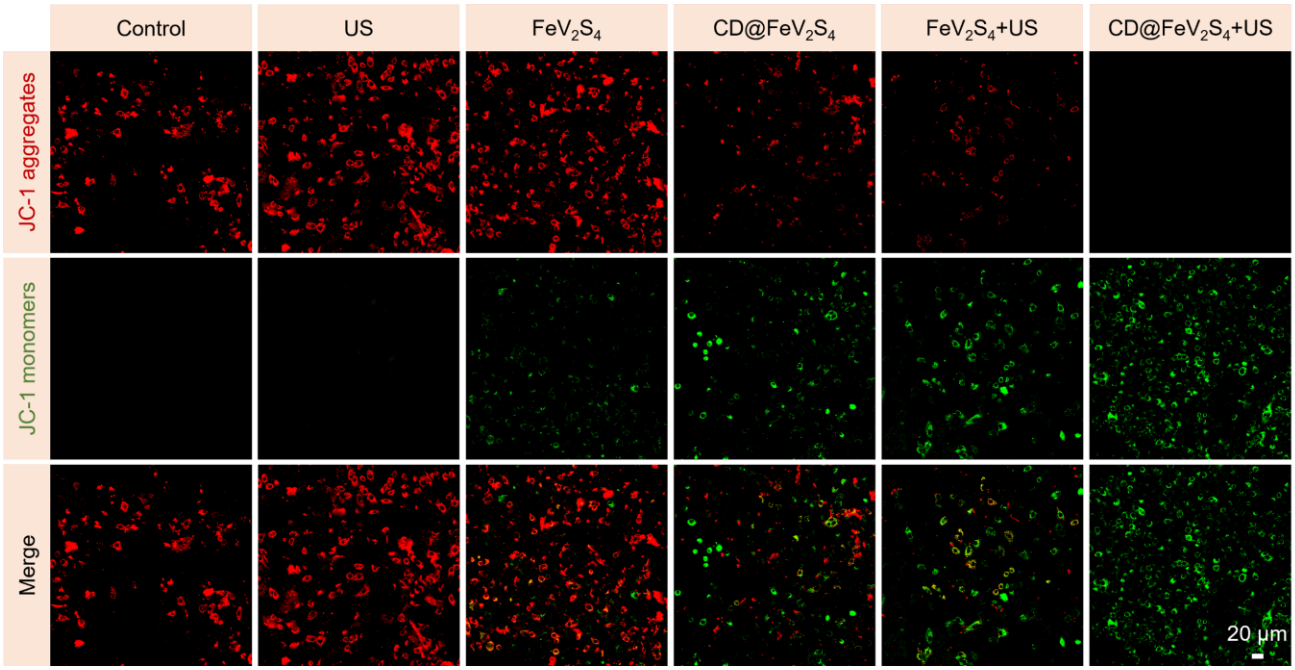


Figure S9. JC-1 staining assay of CT26 cells after different treatments.

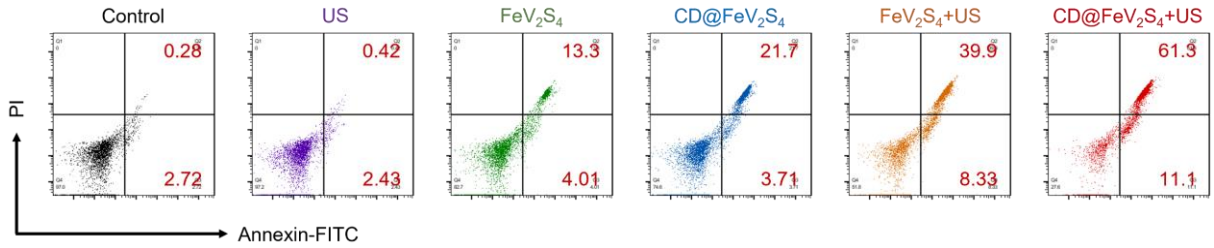


Figure S10. Apoptosis detection assay of CT26 cells after different treatments.

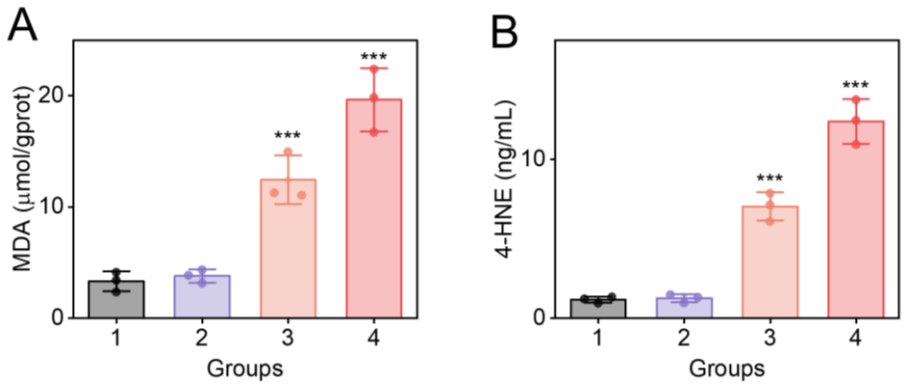


Figure S11. Measurement of the expression level of MDA (A) and 4-HNE (B). Data are presented as the mean ± SD. (n = 3). ***p < 0.001.

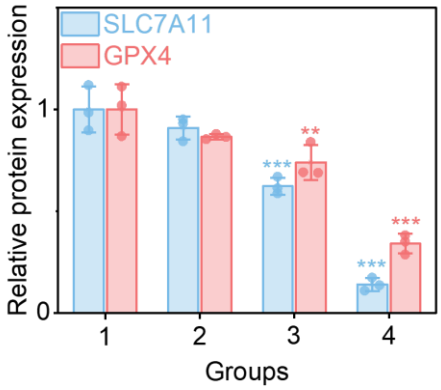


Figure S12. The expression of GPX4 and SLC7A11 after different treatments. Data are presented as the mean ± SD. (n = 5). **p < 0.01, ***p < 0.001.

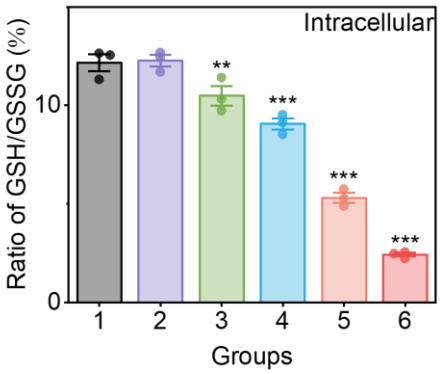


Figure S13. Ratio of GSH/GSSG of CT26 cells after different treatments. Data are presented as the mean ± SD. (n = 3). **p < 0.01 and ***p < 0.001.

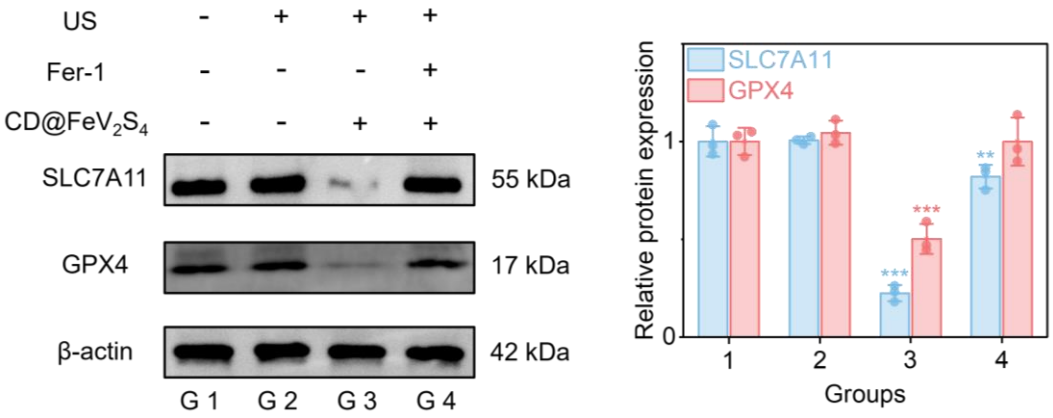


Figure S14. The expression of GPX4 and SLC7A11 after different treatments. Data are presented as the mean ± SD. (n = 5). **p < 0.01 and ***p < 0.001.

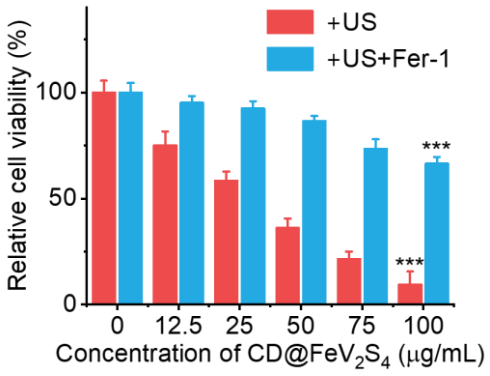


Figure S15. Cytotoxicity assessment of CD@FeV_2S_4 towards CT26 cells under US with or without Fer-1. Data are presented as the mean ± SD. (n = 6). ***p < 0.001.

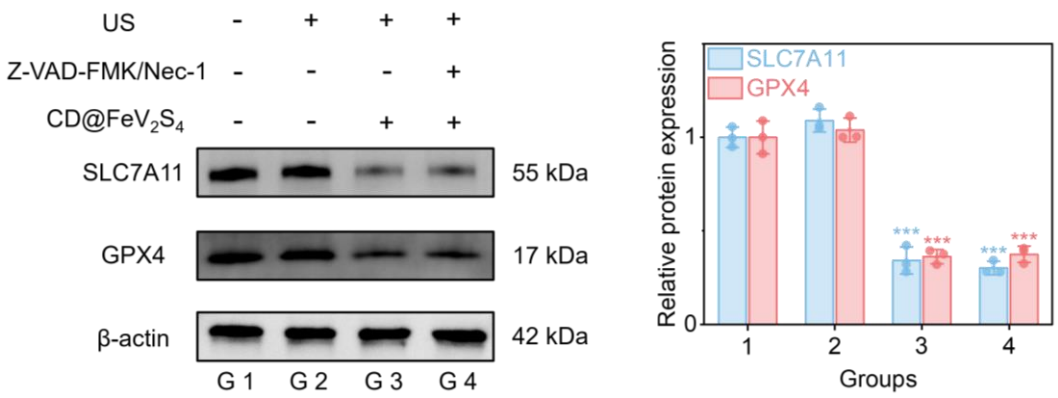


Figure S16. Protein expression levels of GPX4 and SLC7A11 after different treatments. Data are presented as the mean ± SD. (n = 5). ***p < 0.001.

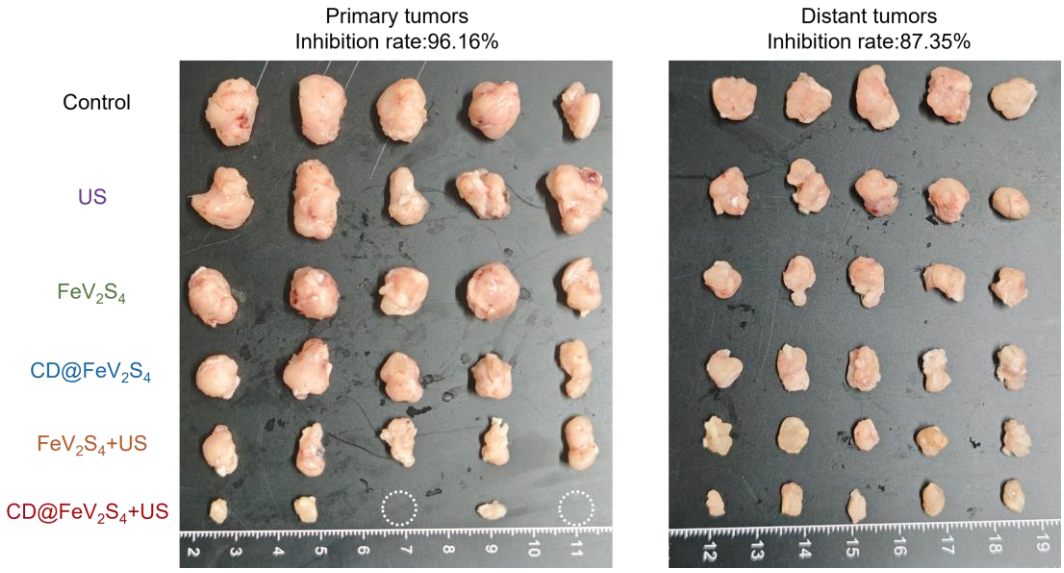


Figure S17. Photographs of the primary and distant tumors in mice after different treatments.

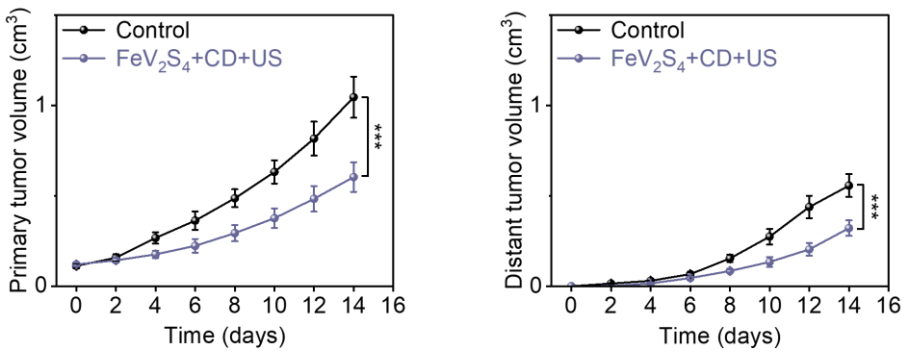


Figure S18. Primary and distant tumor volume of different groups. Data are presented as the mean ± SD. (n = 5). ***p < 0.001.

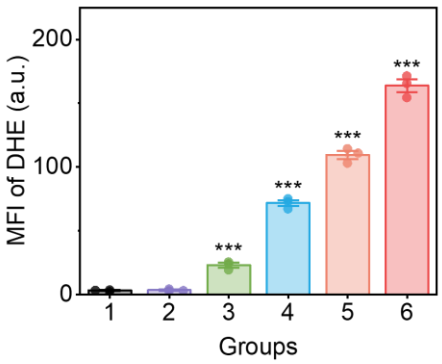


Figure S19. Quantification of DHE fluorescence. Data are presented as the mean ± SD. (n = 3). ***p < 0.001.

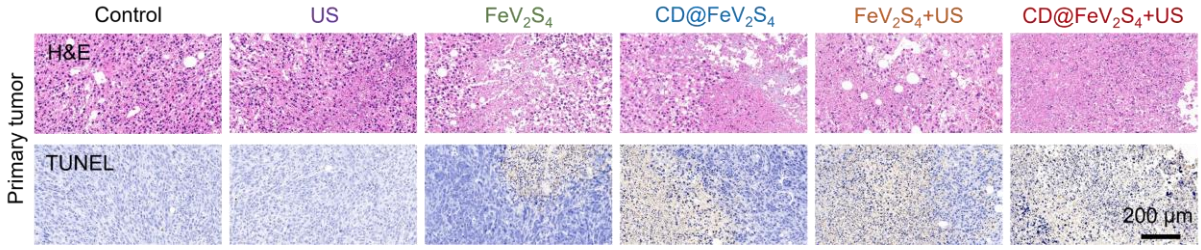


Figure S20. H&E and TUNEL staining in primary tumor tissues after different treatments.

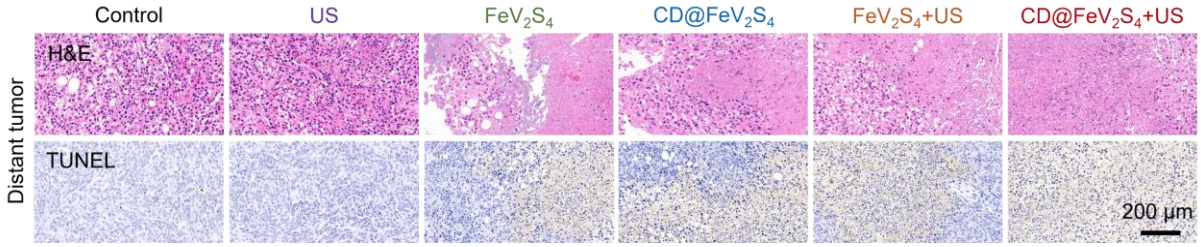


Figure S21. H&E and TUNEL staining in distant tumor tissues after different treatments.

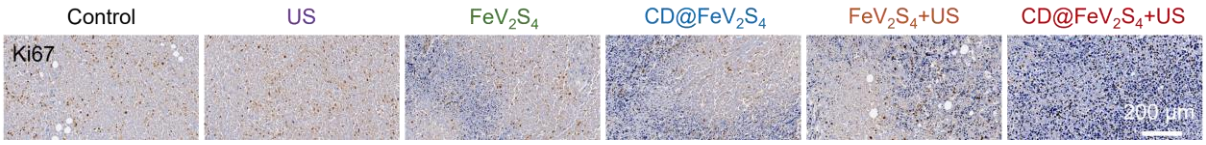


Figure S22. Ki67 staining in primary tumor tissues after different treatments.

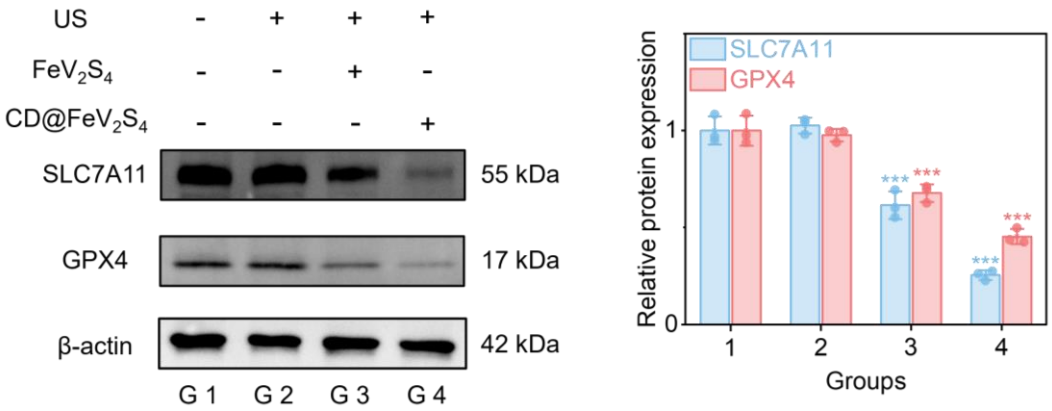


Figure S23. Protein expression levels of GPX4 and SLC7A11 in tumor tissue after different treatments. Data are presented as the mean ± SD. (n = 5). ***p < 0.001.

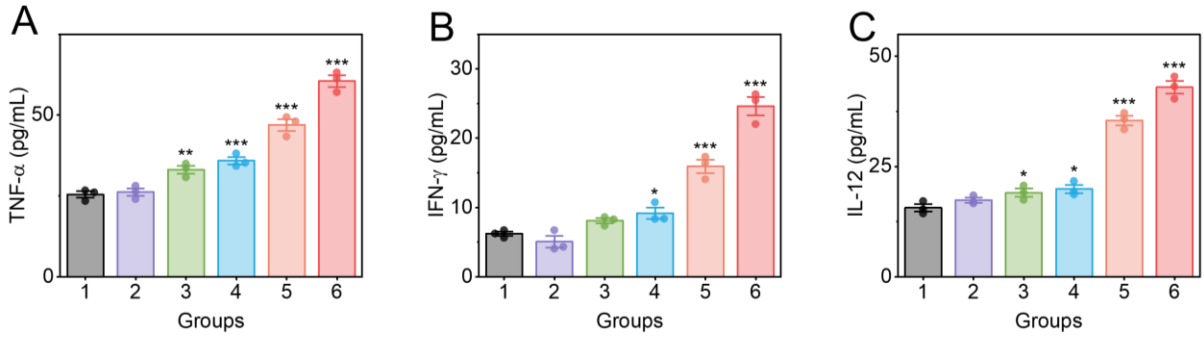


Figure S24. The expression levels of TNF-α (A), IFN-γ (B) and IL-12 (C) in blood serum of mice after different treatments. Data are presented as the mean ± SD. (n = 3). *p < 0.05, **p < 0.01, and ***p < 0.001.

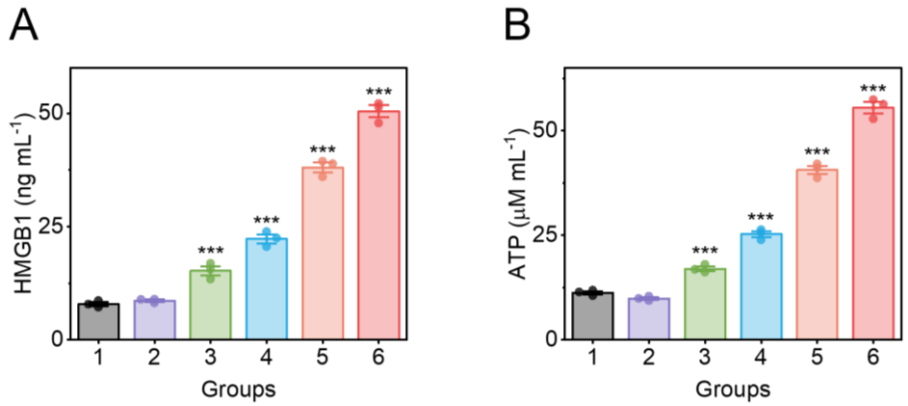


Figure S25. Measurements of HMGB1 (A) and ATP levels (B) in primary tumor tissues after different treatments. Data are presented as the mean ± SD. (n = 3). ***p < 0.001.

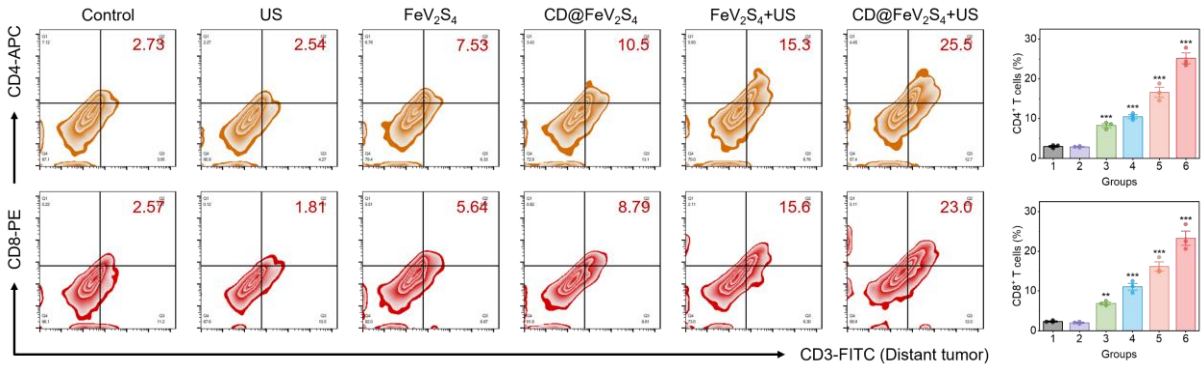


Figure S26. Measurements of the T cell activation level in the distant tumor after different treatments. Data are presented as the mean ± SD. (n = 3). **p < 0.01 and ***p < 0.001.

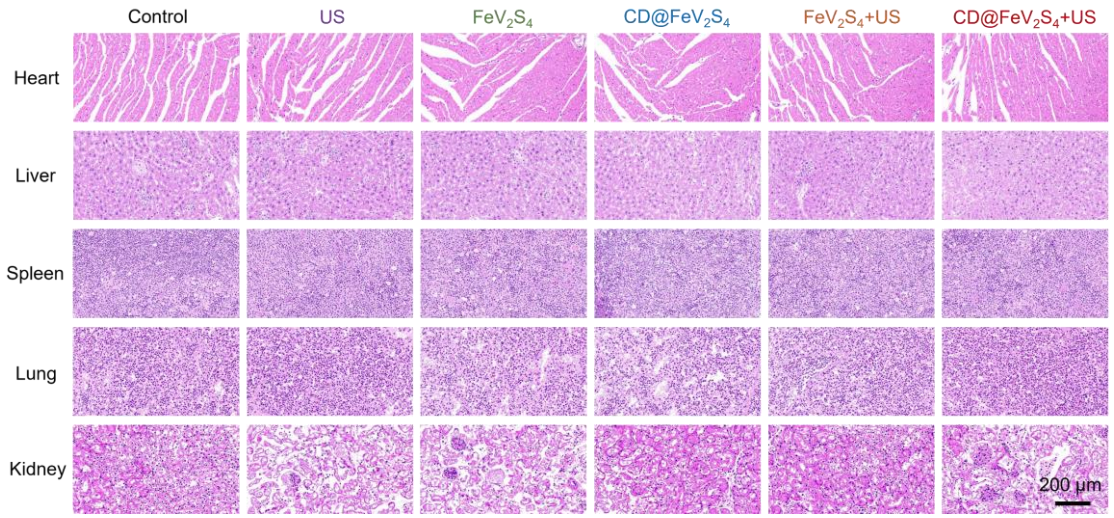


Figure S27. H&E staining of main organs after different treatments.

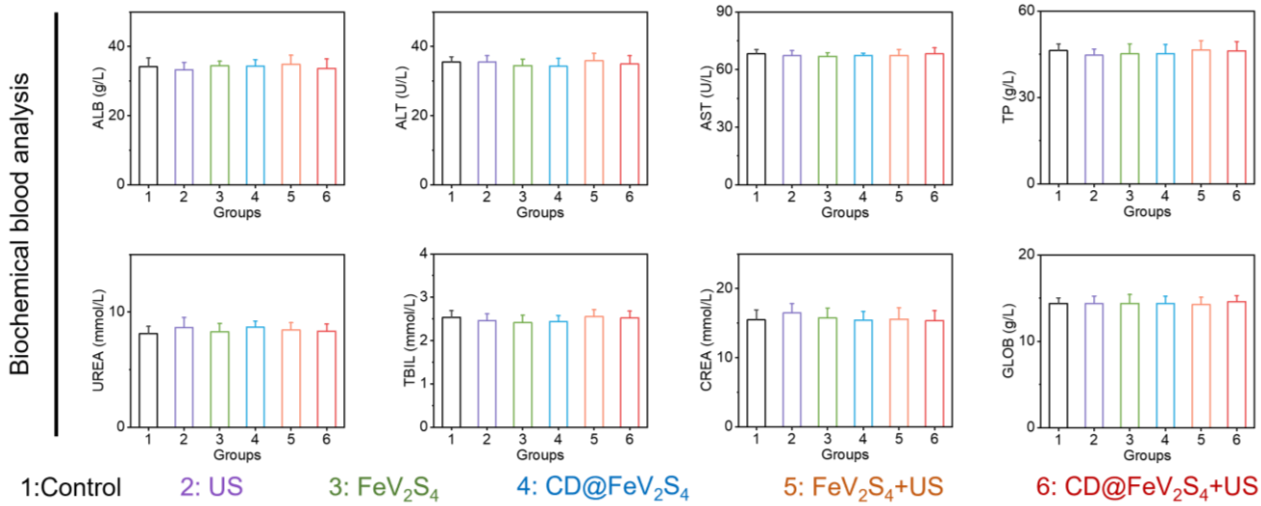


Figure S28. Biochemical blood analysis of mice that were sacrificed at 14 days after different treatments. The terms of biochemical blood analysis include ALT, ALB, AST, TP, UREA, TBIL, CREA,

and GLOB. Data are presented as the mean ± SD. (n = 5).

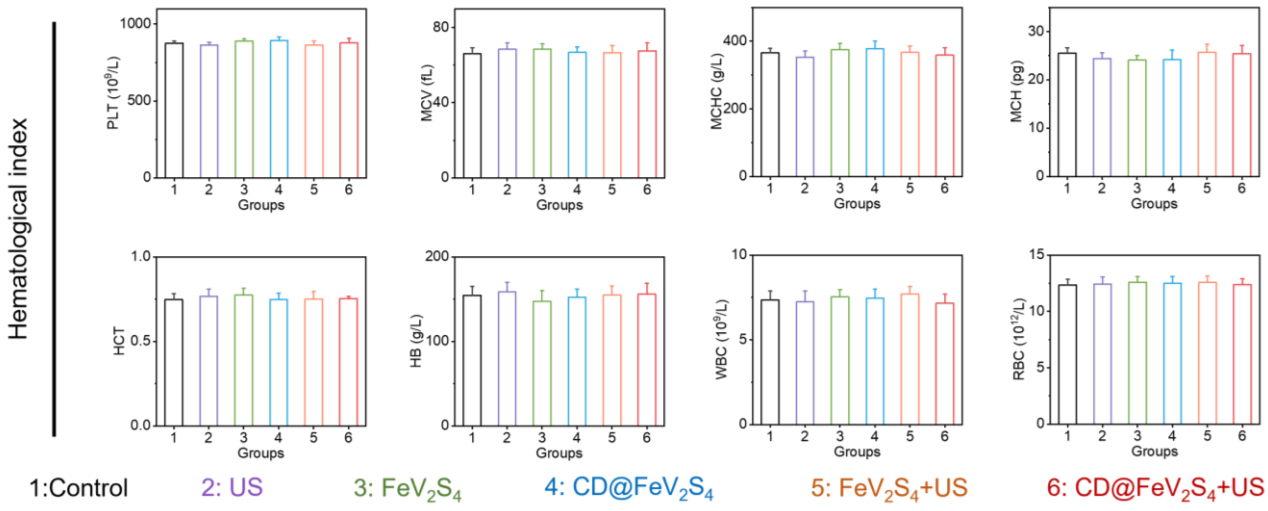


Figure S29. Hematological index of the mice that were sacrificed at 14 days after different treatments. The terms of hematological index include PLT, MCV, MCHC, MCH, HCT, HB, WBC, and RBC. Data are presented as the mean ± SD. (n = 5).

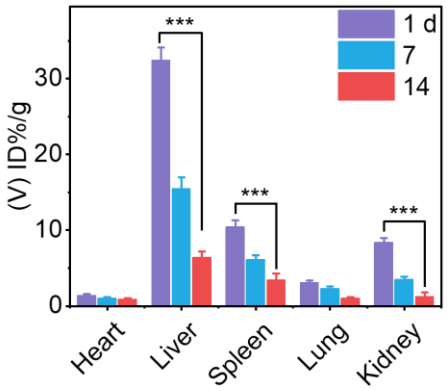


Figure S30. Biodistribution of CD@FeV_2S_4 post i.v. injection in mice on different days. Data are presented as the mean ± SD. (n = 5). ***p < 0.001.

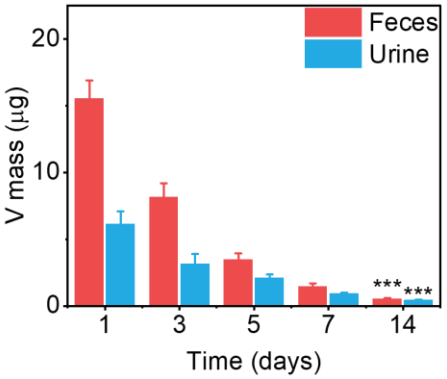


Figure S31. The detected CD@FeV_2S_4 mass in urine and feces at different time points post i.v. injection of CD@FeV_2S_4. Data are presented as the mean ± SD. (n = 5). ***p < 0.001.

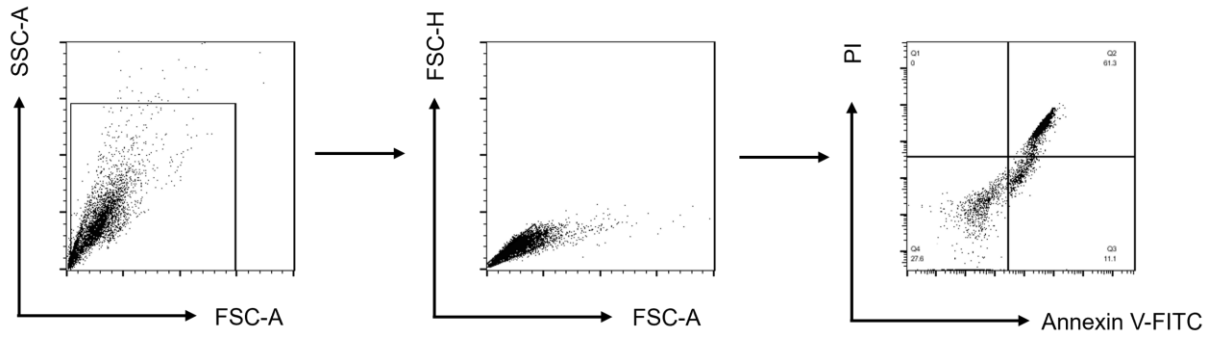


Figure S32. Gating strategy for the flow cytometry analysis of the apoptosis assay in Figure S10.

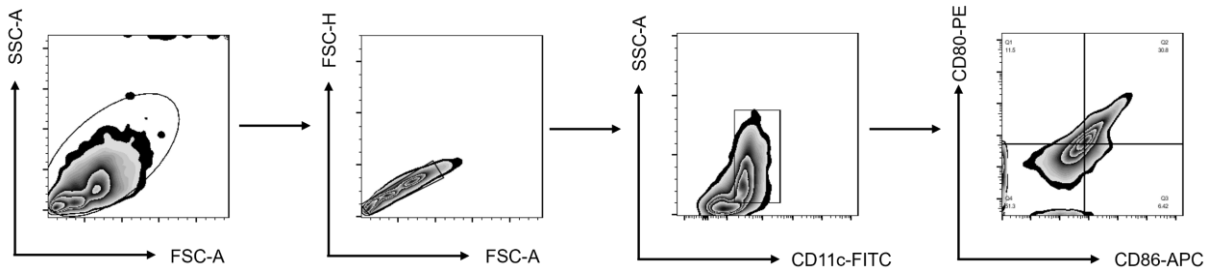


Figure S33. Gating strategy for the flow cytometry analysis of the DC maturation level in Figure 7A.

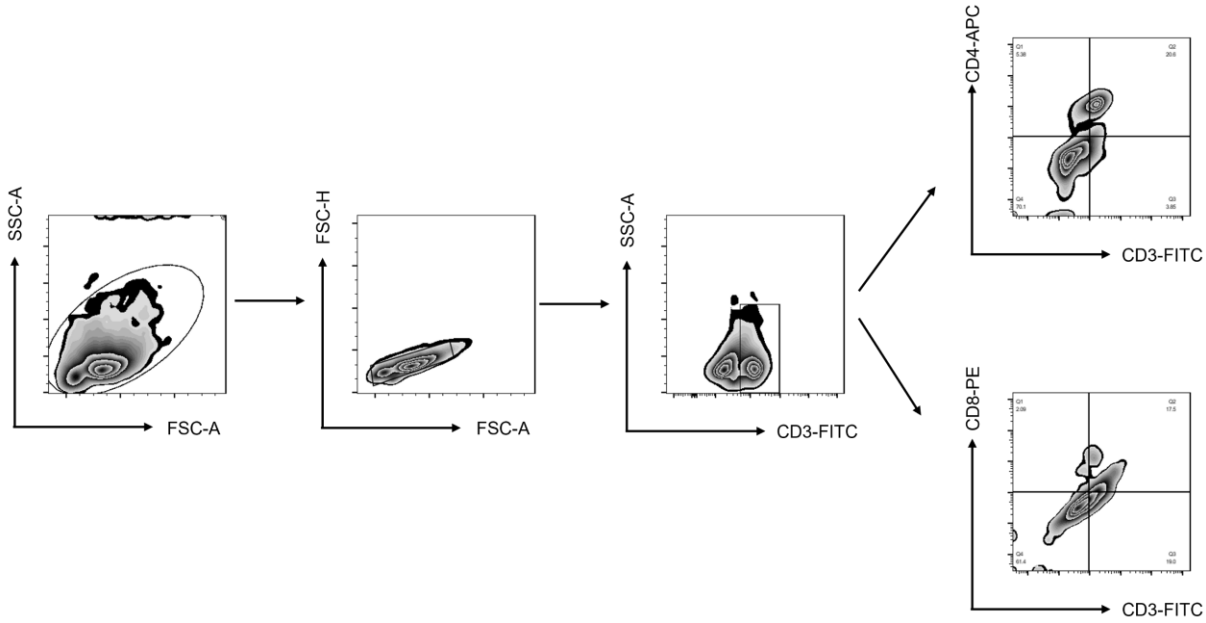


Figure S34. Gating strategy for the flow cytometry analysis of the T cell activation level in Figure 7B.

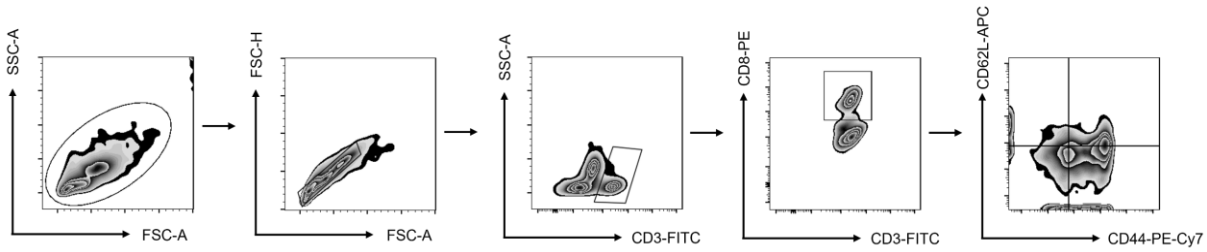


Figure S35. Gating strategy for the flow cytometry analysis of the proportions of $CD3^+CD8^+CD62L^-CD44^+$ effector memory T cells (T_{EM}) in spleen of CT-26 tumor-bearing mice in Figure 8E.